



## Dependence of fracture toughness on multiscale second phase particles in high strength Al alloys

G. Liu, G.-J. Zhang, X.-D. Ding, J. Sun & K.-H. Chen

To cite this article: G. Liu, G.-J. Zhang, X.-D. Ding, J. Sun & K.-H. Chen (2003) Dependence of fracture toughness on multiscale second phase particles in high strength Al alloys, *Materials Science and Technology*, 19:7, 887-896, DOI: [10.1179/026708303225004314](https://doi.org/10.1179/026708303225004314)

To link to this article: <http://dx.doi.org/10.1179/026708303225004314>



Published online: 19 Jul 2013.



[Submit your article to this journal](#)



Article views: 52



[View related articles](#)



Citing articles: 14 [View citing articles](#)

# Dependence of fracture toughness on multiscale second phase particles in high strength Al alloys

G. Liu, G.-J. Zhang, X.-D. Ding, J. Sun and K.-H. Chen

An improved model is described to predict variations in fracture toughness of high strength aluminium alloys with volume fraction, size, and characteristics of the contained multiscale second phases, i.e. ellipse shaped constituents, sphere shaped dispersoids, and disc shaped precipitates, in an integrated manner. Results show that predictions are in broad agreement with values measured experimentally for an aged Al–Cu–Mg alloy. Furthermore, the model was employed to relate the anisotropic fracture toughness of alloy plate to its orientation. A diagram is presented to illustrate the relationship between yield strength and fracture toughness of the aged alloy. MST/5481

Professor Liu, Dr Zhang, Associate Professor Ding and Professor Sun are at the State Key Laboratory for Mechanical Behavior of Materials, School of Material Science & Engineering, Xi'an Jiaotong University, Xi'an, 710049, China (junsun@xjtu.edu.cn). Professor Chen is at the State Key Laboratory for Powder Metallurgy, The University Of Southern Central China, Changsha, China. Manuscript received 4 April 2002; accepted 7 October 2002.

© 2003 IoM Communications Ltd. Published by Maney for the Institute of Materials, Minerals and Mining.

## Introduction

The relatively low fracture toughness of high strength aluminium alloys is a significant limitation to their commercial application. Extensive research has thus been dedicated to examining the dependence of fracture toughness on metallurgical factors in these alloys, with the aim of modifying the factors to improve fracture resistance.<sup>1–11</sup> From these experimental studies, the important metallurgical factors have been determined as: (1) second phase particles, including their volume fraction, dimension, and resistance to cleavage or decohesion; (2) local strain concentration; (3) grain size and morphology; and (4) precipitate free zones (PFZ) that promote intergranular fracture. For common heat treatable aluminium alloys, the latter three factors are essentially associated with second phase particles, especially with dispersoids and precipitates. Thus, second phase particles have traditionally been treated as the dominant factor controlling the fracture resistance of high strength aluminium alloys.

High strength aluminium alloys normally contain three types of second phase particles:<sup>5,7</sup> coarse ellipsoidal constituents, intermediate spherical dispersoids, and fine disc shaped strengthening precipitates. The coarse constituents, normally 1–5 vol.-%, result from the presence of Fe and Si impurities or excessive amounts of major alloying element such as Mg, Zn, and Cu. The final size of constituents depends on the fabrication procedure and may range in diameter from 5 to 30 µm. Dispersoids, with volume fraction 0.05 to 0.2 and having their largest dimension ranging from 0.02 to 0.5 µm, normally precipitate during the ingot preheat and homogenisation treatment. These particles come from the addition of elements of Mn, Cr, Zr, and so on, which are dopants used to control grain size and/or suppress recrystallisation. Dispersoids directly influence the fracture toughness of alloys by affecting crack growth and coalescence. Strengthening precipitates are nanometre sized and form during the aging treatment. They are the major contributor to the strength of alloys and therefore largely control the slip and deformation behaviour and indirectly influence the fracture toughness of the alloys.

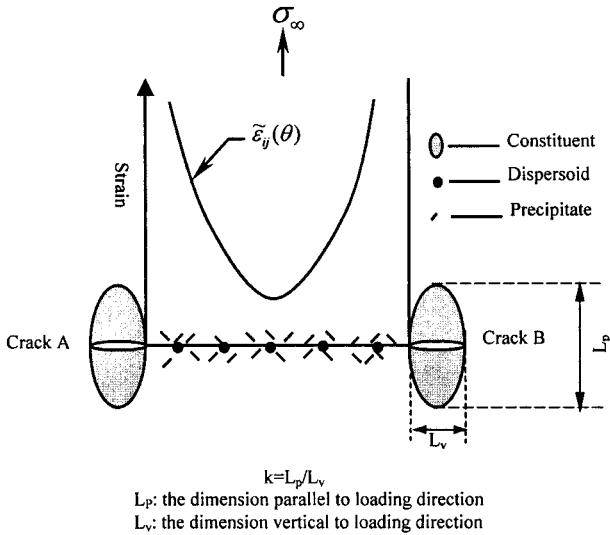
It is well known that brittle constituents are crack initiators or form preferential crack paths because they are prone to cleavage or they separate from the matrix. Accordingly, they are detrimental to the fracture toughness

of aluminium alloys. Many experimental results have shown that lowering the iron and silicon levels and hence the volume fraction of constituents increases the fracture toughness of high strength aluminium alloys<sup>6,12</sup> and this principle has been employed to assist the development of 2124, 7050, 7175, and 7475 aluminium alloys. As a theoretical aid, some equations have been proposed for relationships among fracture toughness and volume fraction, mean diameter, and interparticle spacing of constituents,<sup>8,13</sup> and these analytical relationships have been partially validated experimentally.<sup>8,14</sup> However, the influence of smaller second phase particles, i.e. dispersoids and precipitates, on fracture toughness have not been presented in quantitative terms, although they are also significant. The reason for this is the distinct difference (~100 times) in the dimensions of these three types of second phase particles, which makes coupling their influence on fracture toughness into an integrated model rather difficult.

For alloys containing multiscale microstructure features, modelling quantitatively the non-linear relationship between microstructure and macroductility and fracture toughness has been done, based on major microstructure features and ignoring partially or completely other scale microstructure features. This was because of the difficulty of coupling multiscale microstructure features within a continuous medium and determining their contribution to macroplastic and fracture toughness properties. Thus only the major contributor was considered. Modelling the dependence of fracture toughness of high strength aluminium alloys on multiscale second phase particles would fail in this case.

Recently, interest has been focused on the multiscale modelling of polycrystal plasticity,<sup>15</sup> failure in metal matrix composites,<sup>16</sup> and mechanical response of alloys or composites<sup>17,18</sup> using finite element based approaches and adopting mechanism based strain gradient plasticity theory,<sup>19–26</sup> Green's function methods,<sup>27,28</sup> and image processing,<sup>29,30</sup> jointly or separately. Investigations into the size effect of second phase particles on plasticity of metals and their alloy or metal matrix composites has also been undertaken.<sup>31</sup>

This has motivated the present work, in which we try to integrate the influences of three kinds of second phase particles on fracture toughness into an improved analytical model for high strength aluminium alloys. Subsequently we use this fracture toughness model together with an established precipitation and strengthening model<sup>32</sup> to present an overall description of the yield strength and fracture



1 Scheme illustrating local fracture behaviour in heat treatable high strength aluminium alloys

toughness with aging of heat treatable aluminium alloys containing multiscale second phase particles, and then validate it experimentally.

**Model**

**TENSILE DUCTILITY MODEL**

As observed in practice, brittle constituents will fracture readily during processing or under service loading, so it is reasonable to treat them as microcracks directly (Fig. 1). Assuming these microcracks arrange in a cubic array, the macroplastic strain of specimens  $\epsilon$  could be obtained analytically from microplastic strain  $\tilde{\epsilon}$  as follows<sup>33</sup>

$$\epsilon = \frac{1}{\tilde{\epsilon}_n(\theta)} \left[ \frac{I}{0.405\pi h} \right]^{\frac{1}{n+1}} \left[ \frac{\lambda_c}{2r_c} - 1 \right]^{\frac{1}{n+1}} \frac{\tilde{\epsilon}}{2} \quad (1)$$

where  $\lambda_c$  and  $r_c$  are interparticle spacing and radius of constituents, respectively,  $\tilde{\epsilon}_n(\theta)$  is the effective value for normalised coefficient  $\tilde{\epsilon}_{ij}(\theta)$ ,<sup>34,35</sup> and is a constant for  $\theta=0$ ,  $I$  and  $h$  are functions of  $n$ <sup>36-38</sup>

$$I = 10.3\sqrt{0.13+n} - 4.8n \quad (2)$$

$$h = \frac{3}{2\sqrt{1+3n}} \quad (3)$$

$\tilde{\epsilon}$  is critical local strain at the middle of the ligament connecting two neighbouring microcracks. It is also equivalent to the minimum strain required to promote void/microcrack growth and coalescence up to instability. Those dispersoids and precipitates distributed in the ligament dominate this damage evolution process, and morphological demonstrations such as void sheets and/or slip bands are readily observed on the fracture surfaces or sectioned profiles of broken specimens.

In tensile condition, aluminium matrix will undergo plastic deformation, while the nearly pure elastic second phase particles maintain their shape: this incompatibility in shape change incurs geometrically necessary dislocations which are introduced to make up for the discrepancy.<sup>39</sup> The densities  $\rho_d$  and  $\rho_p$  of geometrically necessary dislocations around dispersoids and precipitates are determined by the strains exerted on the adjacent matrix bonded with the two populations of particles,  $\epsilon_d$  and  $\epsilon_p$  respectively<sup>39,40</sup>

$$\epsilon_d = 1.7r_d b \rho_d \quad (4a)$$

$$\epsilon_p = 0.25\lambda_p b \rho_p \quad (4b)$$

with  $r_d$  the radius of the dispersoids,  $\lambda_p$  the interparticle

spacing of precipitates, and  $b$  Burgers vector of the matrix. According to Ashby,<sup>39</sup> the ratio between  $\rho_d$  and  $\rho_p$  is associated with the ratio between interparticle spacing of the two populations of particles  $\lambda_d$  and  $\lambda_p$  as follows

$$\frac{\rho_d}{\rho_p} = k \frac{\lambda_p}{\lambda_d} \quad (5)$$

where  $k$  is a scaling factor and set to unity here. Letting  $\rho_g$  be the sum of  $\rho_d$  and  $\rho_p$ , equation (5) can be expressed in the form

$$\rho_d = \frac{\lambda_p}{\lambda_d + \lambda_p} \rho_g \quad (6a)$$

$$\rho_p = \frac{\lambda_d}{\lambda_d + \lambda_p} \rho_g \quad (6b)$$

The density  $\rho_g$  of geometrically necessary dislocations, plus the density of statistically stored dislocations  $\rho_s$  gives the total dislocation density of the matrix  $\rho_t$

$$\rho_t = \rho_g + \rho_s \quad (7)$$

A critical value of  $\rho_t$  denoted  $\rho_t^c$ , is assumed to exist and once  $\rho_t$  reaches this 'dislocation limit', the material fractures regardless of what the detailed mechanism is. Neglecting constraints from second phase particles,  $\rho_t^c$  should be a constant if the following engineering mechanical expression could be applied effectively to the microscale ligament

$$\tau_m = \alpha G b \sqrt{\rho_t^c} \quad (8)$$

in which  $\tau_m$  is the intrinsic shear strength of the matrix,  $G$  is the shear modulus of the matrix,  $b$  and  $\alpha$  are constants for a given matrix such as aluminium. At the same time  $\rho_s$  could be considered approximately invariant by reasoning that the increase in  $\rho_s$  is very inappreciable compared with that in  $\rho_g$  under external loading.<sup>41</sup> Therefore the criterion for fracture is further defined as

$$\rho_g^c = \rho_t^c - \rho_s \quad (9)$$

From the above analyses, equation (4) can be rewritten as

$$\epsilon_d^c = 1.7r_d b \frac{\lambda_p}{\lambda_d + \lambda_p} \rho_g^c \quad (10a)$$

$$\epsilon_p^c = 0.25\lambda_p b \frac{\lambda_d}{\lambda_d + \lambda_p} \rho_g^c \quad (10b)$$

where  $\epsilon_d^c$  and  $\epsilon_p^c$  are critical strains at fracture, relevant to the dispersoids and precipitates, separately.

$\tilde{\epsilon}$  in equation (1) is a combination of  $\epsilon_d^c$  and  $\epsilon_p^c$  in the form of a Pythagorean theorem, not of linear addition, due to the overlap effect between the two types of strains

$$\tilde{\epsilon} = \sqrt{(\epsilon_d^c)^2 + (\epsilon_p^c)^2} \quad (11)$$

Thus the strain to fracture of aluminium alloys could be obtained as

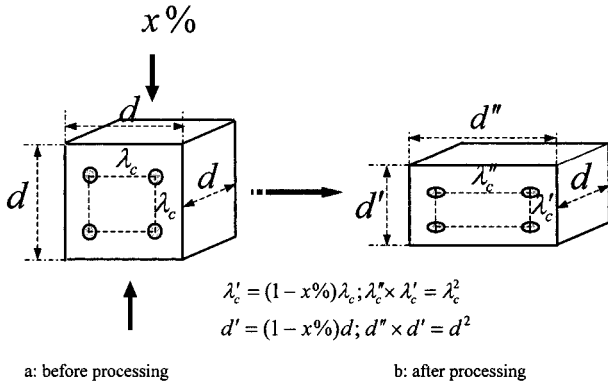
$$\epsilon = \frac{1}{\tilde{\epsilon}_n(\theta)} \left[ \frac{I}{0.405\pi h} \right]^{\frac{1}{n+1}} \left[ \frac{\lambda_c}{2r_c} - 1 \right]^{\frac{1}{n+1}} \frac{\sqrt{(\epsilon_d^c)^2 + (\epsilon_p^c)^2}}{2} \quad (12)$$

**FRACTURE TOUGHNESS MODEL**

Based on the criterion that fracture will occur when the local strain ahead of the main crack exceeds the critical value  $\epsilon_c^*$ , an expression has been established to relate the fracture toughness of high strength aluminium alloys to yield strength  $\sigma_y$ , strain hardening exponent  $n$ , Young's modulus  $E$ , and  $\epsilon_c^{*10}$

$$K_{IC} = \sqrt{\frac{2CE\epsilon_c^*\sigma_y n^2}{(1-\nu^2)}} \quad (13)$$

where  $C$  is a constant  $\approx 1/40$  and  $\nu$  is Poisson's ratio. As for



**2 Sketch illustrating influence of deformation in processing on dimensional change of grains and constituents**

equation (1), although  $\epsilon_c^*$  is (qualitatively) known to be a function of the volume fraction  $f_c$  of void initiating constituents,<sup>3</sup> i.e.

$$\epsilon_c^* = f \left( \frac{1}{f_c} \right) \dots \dots \dots (14)$$

no explicit solution has been put forward, even though only this one kind of second phase particle is taken into account. Thus, this current modelling will try to make an improvement to integrate the influences from the three kinds of second phase particles into the fracture toughness predicting expression.

Earlier we derived the engineering tensile ductility  $\epsilon$  as equation (12). It has been suggested<sup>42</sup> that  $\epsilon_c^*$  in equation (13), i.e. the critical local strain ahead of main crack, was probably half of the true strain  $\epsilon$  in the tensile test, and some experimental results<sup>10</sup> have supported this as a reasonable first approximation. According, we can substitute  $\epsilon_c^* = \frac{1}{2} \epsilon$  and equation (12) into equation (13) to obtain the final expression for fracture toughness

$$K_{IC} = A \sqrt{Bn^2 \sigma_y \left[ \frac{\lambda_c}{2r_c} - 1 \right]^{\frac{1}{n+1}} [(1.7r_d \lambda_p)^2 + (0.25 \lambda_p \lambda_d)^2]^{1/2} (\lambda_d + \lambda_p)^{-1}} \quad (15)$$

with

$$A = \sqrt{\frac{cE}{2\bar{\epsilon}_n(\theta)}} \dots \dots \dots (16)$$

$$B = [(1 + 3n)(5.39\sqrt{0.13 + n} - 2.53n)]^{\frac{1}{n+1}} \dots \dots \dots (17)$$

For a cubic array, the volume fraction of second phase particles  $f_i$  ( $i = c, d, p$ ) is a function of the mean radius  $r_i$  ( $i = c, d, p$ ) and the interparticle spacing  $\lambda_i$  ( $i = c, d, p$ )

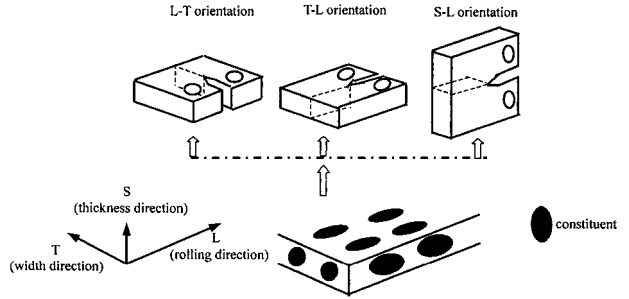
$$f_i = 2\pi k \left( \frac{r_i}{\lambda_i} \right)^3 \dots \dots \dots (18)$$

where  $k$  is the aspect ratio of second phase particles and is 1 for spherical dispersoids. For disc shaped precipitates,  $k$  is defined as the ratio between the radius of the plate plane and the half height of the disc, and is chosen as 40 in the present work.

Defining  $(K_{IC})_R$  as a reference fracture toughness, yields the normalised fracture strain  $R_{ft}$  by dividing  $K_{IC}$  by  $(K_{IC})_R$

$$R_{ft} = \frac{K_{IC}}{(K_{IC})_R} \dots \dots \dots (19)$$

If we regard the as quenched condition as the reference case, i.e. the fracture toughness of as quenched specimens is the reference value, or if we regard the absence of any kind of second phase particle as the reference case, then the relative change of fracture toughness of aluminium alloys with aging as well as with variation of any kind of second phase particle in size, volume fraction, and morphology, can be



**3 Sketch illustrating contribution of constituents to orientation effect of fracture toughness of aluminium alloy plate**

represented by equation (19). This is done by changing the parameters of one kind of second phase particle, but keeping the parameters of the two other kinds of second phase particles unchanged.

It must be noted that, for constituent particles, the cubic array assumption for constituents employed in equation (18) falls short of industrial actuality, where the constituents do not arrange in an equal sided cubic manner. Referring to Fig. 2, before processing, the constituents in as cast aluminium alloys are distributed homogeneously and are spherical in shape due to the minimum surface energy effect during forming. During processing, deformation from rolling or pressing the cell makes thin plates with the dimension parallel to the direction of the outside force reduced. At the same time, the interparticle spacing of constituents changes in an analogous fashion. If the deformation is  $x\%$ , the plate thickness and vertical interparticle spacing of constituents will decrease to  $(1 - x\%)$  of their former values. Now the  $\lambda_c$  in equation (15) should be replaced by  $(1 - x\%) \lambda_c$  for L-T orientation fracture toughness (Fig. 3). Provided the dimension along the width is unaltered both for the cell and for interparticle spacing of constituents in the course of processing, the length of the cell and the horizontal interparticle spacing of constituents will increase by  $\frac{1}{1 - x\%}$  assuming a constant volume. At the same time, if we regard the cell as a grain and the bulk plate specimen as being a pile up of similarly shaped cells, then it can be concluded that the fraction along the grain boundary is greatest in the direction perpendicular to the thickness, or the S direction (Fig. 3). Furthermore, the shape of constituents will change from spherical to ellipsoidal with axis parallel to the rolling or pressing direction. These are all contributors to the orientation effect in the fracture toughness of aluminium alloy plates and details will be discussed below.

**Experimental procedure**

The Al-Cu-Mg alloy plate used here was supplied by Research laboratory of Xi'an Aircraft Industry Ltd, and is 16 mm thick, hot rolled plate with a measured composition (wt-%) of Al: balance, Cu: 4.62, Mg: 0.65, Mn: 0.22, Si, Fe, Zn < 0.30. A T-6 heat treatment was employed for this material including solution treatment at 766 K for 2 h then quenched into flowing water, and subsequently aged at 513 K for various times from 0.25 h to 10 days.

Because the present Al-Cu-Mg alloy plate and the Al-Cu-Mg alloy rod used for measuring yield strength<sup>32</sup> are from the same ingot, and the former possesses nearly the same tensile property in the L direction as the latter, the fracture toughness was determined for the Al-Cu-Mg alloy plate.

The fracture toughness was characterised with compact tension (CT) specimens and the R curve method. Both L-T and T-L orientated specimens were machined for

comparison, each with a width of 62.5 mm and thickness 6.25 mm. Specimens were fatigue cracked prior to fracture toughness experiments, at a constant stress ratio ( $R = K_{min}/K_{max}$ ) of 0.1 and under decreasing stress intensity conditions. Fracture toughness experiments were performed on a servo-hydraulic Instron-type testing machine strictly conforming to ASME 561, using a potential drop methodology to measure crack length. The measured data were analysed to determine plane strain fracture toughness at crack initiation.<sup>43</sup>

The microstructure of Al-Cu-Mg alloy plate was examined using optical microscopy. Metallographic preparation involved normal procedures using a series of abrasive papers, diamond pastes, and final polishing with a slurry made of reagent grade MgO and distilled water. The specimens were etched by immersion into Keller's etchant.

Constituent volume fraction measurements were made at a magnification of 400 using a grid containing 900 points. Six random views on each of three specimens per alloy were examined. The distribution of the constituents within each alloy was assumed to be random, therefore the volume fraction  $V_c$  is given by  $P_p$ , which is the fraction of total grid points that fall on constituent particles. Constituents smaller than 0.1  $\mu\text{m}$  were not measured.

Constituent radius measurements were performed using a HITACHI S-2700 scanning electron microscope on sectioned profiles of the untested rod shaped specimens. Since the constituents are irregular in shape, an effective particle diameter  $d_c$  is defined as

$$d_c = \sqrt{d_1 d_2} \dots \dots \dots (20)$$

where  $d_1$  and  $d_2$  are the smallest and largest dimensions of a constituent, respectively. The average effective constituent radius  $\bar{r}_c$  of  $n$  particles is given by

$$\bar{r}_c = \frac{\sum_{i=1}^n \sqrt{d_1 d_2}}{2n} \dots \dots \dots (21)$$

To obtain the value of  $\bar{r}_c$  for each alloy, at least 50 constituents were measured in each of three sectioned specimens.

Dispersoid radius was determined by the same methods using a JEOL Ltd. JEM-200CX transition electron microscope operating at 100 kV. The preparation of foils for TEM examination has been described elsewhere.<sup>32</sup> The volume fraction of dispersoids is related to the average effective radius by<sup>44</sup>

$$V_d = \frac{4(\pi \bar{r}_d^3)}{3} \bar{N}_d \dots \dots \dots (22)$$

The particle density  $\bar{N}_d$  is defined as<sup>45</sup>

$$\bar{N}_d = \frac{N_d}{(t + 2\bar{r}_d)} \dots \dots \dots (23)$$

where  $t$  is the foil thickness and is easily obtained utilising convergent beam electron diffraction patterns,<sup>46</sup>  $N_d$  is the number of dispersoids per unit area of projected image.

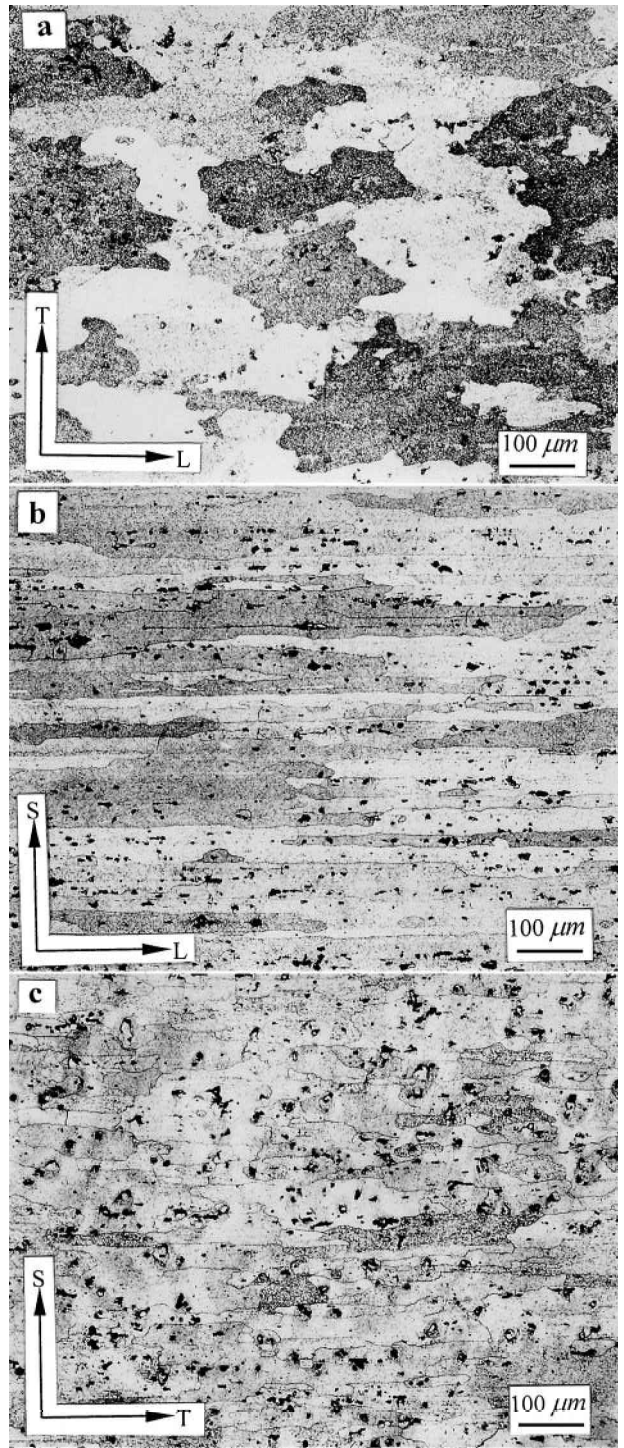
Observations of fracture surfaces of broken specimens were carried out using SEM in order to examine the evolution of void sheets with aging, especially the evolution of the radius of little dimples in void sheets, which can indicate a decohesion condition in the dispersoid.

Measurement of precipitates has been addressed in detail elsewhere,<sup>32</sup> and is not repeated here.

**Results and discussion**

**INFLUENCES OF CONSTITUENTS ON FRACTURE TOUGHNESS**

Typical triplanar optical micrographs of the Al-Cu-Mg plate are shown in Fig. 4. The quantitative metallography



a L-T plane; b L-S plane; c T-S plane

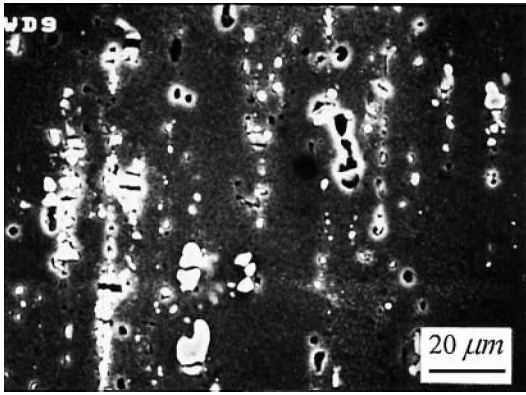
**4 Triplane of Al-Cu-Mg alloy exhibiting the three microstructures**

measurements for both size and volume fraction of constituents and dispersoids are listed in Table 1.

It is well known that brittle constituents are initiators for voids. On the one hand, they break easily when bulk

**Table 1 Volume fraction and radius of constituents and dispersoids in this present experiment**

Alloy	Constituents		Dispersoids	
	$V_c$ (%)	$r_c$ ( $\mu\text{m}$ )	$V_d$ (%)	$r_d$ ( $\mu\text{m}$ )
Al-Cu-Mg	4.83	4.1	0.18	0.08



5 SEM micrographs illustrating fracture or decohesion of constituents in test Al-Cu-Mg alloys

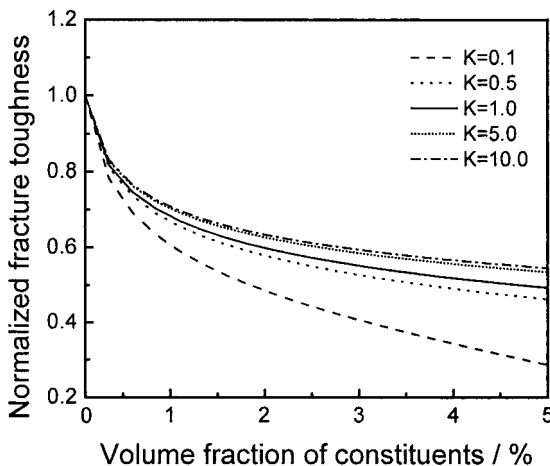
material is subjected to large strains during processing. On the other hand, they fracture readily under service loading. If we consider the aluminium alloys as composites consisting of only the ‘equivalent’ aluminium matrix and constituents, we can express the tensile stress ( $\sigma_s$ ) of the composite as

$$\sigma_s = V_c \sigma_c + (1 - V_c) \sigma_m \dots \dots \dots (24)$$

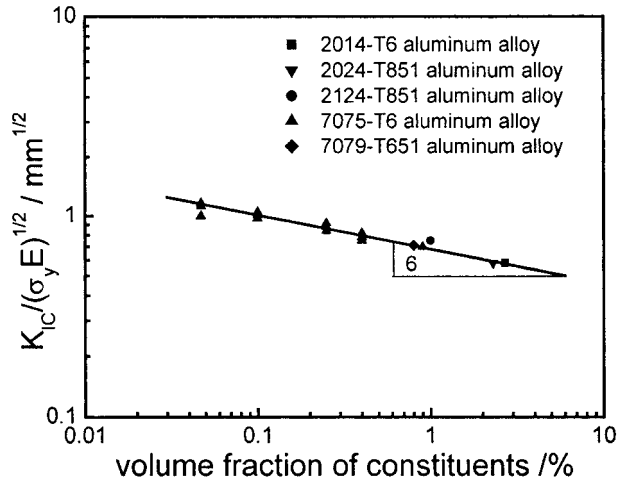
where  $\sigma_c$  and  $\sigma_m$  are stresses undergone by constituents and matrix, respectively,  $V_c$  is the volume fraction of constituents. Due to the small value of  $V_c$  ( $\sim 0.05$ ), even if  $\sigma_c$  reaches the fracture strength of constituents ( $\sigma_c^*$ ), its contribution to  $\sigma_s$  is not prominent. In contrast, exerting a stress  $\sigma_s$ , which is much smaller than  $\sigma_c^*$ , on a specimen can cause most of the constituents to be cleaved or separated from the matrix due to high levels of stress triaxiality or hydrostatic stress,<sup>47-50</sup> as shown in Fig. 5. It is therefore concluded that lower purity, or more constituents will degrade the fracture toughness of aluminium alloys, as depicted in Fig. 6. Thus, purification is an effective approach to improve the deformation capacity and fracture resistance. In addition, smaller constituents are less prone to crack because a greater value is required for the critical fracture stress  $\sigma_c^*$  to trigger cracking<sup>51</sup>

$$\sigma_c^* = \left( \frac{6\gamma E}{q^2 d} \right)^{1/2} \dots \dots \dots (25)$$

where  $d$ ,  $E$ , and  $\gamma$  are the diameter, Young’s modulus, and surface energy of the constituents, respectively, and  $q$  is the stress concentration factor at the particles. For example,  $\sigma_c^*$  of constituents in AA 2024 increases from 540 to 740 MPa with decreasing particle diameter.<sup>52</sup>



6 Modelled dependence of fracture toughness on volume fraction and aspect ratio of constituents



7 Influence of volume fraction of constituents on fracture toughness of high strength aluminium alloys<sup>8</sup>

In a pioneering model, an equation has been proposed to relate the fracture toughness to the volume fraction of void initiating constituents  $f_c$  for aluminium alloys<sup>8</sup>

$$K_{IC} = \left[ 2\sigma_y E \left( \frac{\pi}{6} \right)^{1/3} r_c \right]^{1/2} f_c^{-1/6} \dots \dots \dots (26)$$

Equation (26) was generally accepted for accurately predicting the relationship  $K_{IC} / \sqrt{\sigma_y E} \propto f_c^{-1/6}$ , which was in good agreement with experiments, as shown in Fig. 7.<sup>8</sup> Nevertheless, the shortcomings of equation (26), showing truth disobedient unidirectional change trends between  $K_{IC}$  with  $\sigma_y$  and radius of constituents  $r_c$ , restricted its reliability. Subsequently, a model was suggested to ameliorate these shortcomings to some extent by incorporating  $n$ , which is in inverse variation with  $\sigma_y$ , into the model and to establish an experiment consistent expression for  $K_{IC} \propto n \sqrt{\sigma_y}$ . This failed to take into account the effects of second phase particles directly (refer to equation (13)).<sup>10</sup> The proposed model, improved from the earlier model, not only inherits its merits, but also is essentially identical with that of Hahn and Rosenfield in its advantages, as proved in the following.

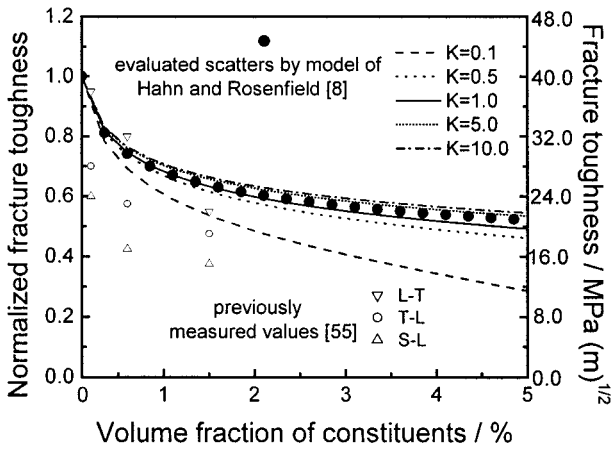
From equation (26), a simplified form is obtained

$$\frac{K_{IC}}{\sqrt{\sigma_y E}} \propto \left[ \frac{\lambda_c}{2d_c} - 1 \right]^{\frac{1}{2(n+1)}} \dots \dots \dots (27)$$

Substituting equation (18) into equation (27) leads to

$$\frac{K_{IC}}{\sqrt{\sigma_y E}} \propto \left[ \left( \frac{2\pi k}{f_c} \right)^{1/3} - 1 \right]^{\frac{1}{2(n+1)}} \dots \dots \dots (28)$$

Because the value of  $n$  is small ( $\sim 0.15$ ), the superscript in equation (28) can be taken as  $1/2$ . If the loading direction is parallel to the long axial direction, as when testing the L-T orientation plain strain fracture toughness for plate specimens (Fig. 3),  $k$  is large enough to make the second part inside the square brackets in equation (28) negligible, hence giving the same conclusion as obtained in equation (26). If the loading direction is parallel to the short radial direction, as when testing the T-L and S-L orientation plain strain fracture toughness of plate specimens,  $k$  is much less than unity and the same conclusion is not obtained. Obviously, it can be inferred that the  $K_{IC}$  of T-L and S-L orientated specimens are less than the counterpart of an L-T orientated specimen because the former have greater values of  $k$ , which is in accordance with experimental results.<sup>5,53,54</sup> These conclusions are clearly revealed in Fig. 8, which presents the dependence of fracture toughness on volume fraction and shape factor of constituents for aluminium alloys from previous<sup>55</sup> and present measured values, and modelling



**8 Contribution of aspect ratio of constituents to orientation effect of fracture toughness of aluminium alloy plate**

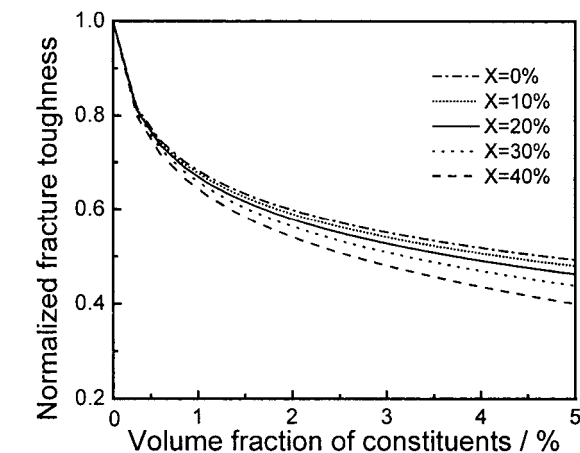
using equation (26), and the current modelling. It is shown that a similar change trend exists for both the modelled results and experimental results and the essential features of equation (26) are embodied in the current model.

In addition, the S-L orientation fracture toughness is less than the T-L case.<sup>5,55</sup> This is associated with the propagating path of a crack. It is well known that the fracture of aluminium alloys arises from intragranular fracture and intergranular fracture,<sup>56-58</sup> and fracture toughness is expressed as a linear sum of the two parts<sup>59,60</sup>

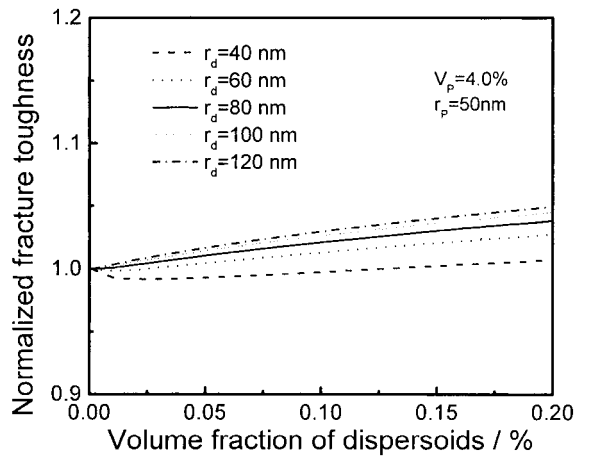
$$K_{IC} = A_{inter} K_{IC}^{inter} + A_{intra} K_{IC}^{intra} \dots \dots \dots (29)$$

where  $K_{IC}^{inter}$  and  $K_{IC}^{intra}$  are the fracture toughness for intergranular and intragranular fracture, respectively,  $A_{inter}$  and  $A_{intra}$  are the fraction of intergranular and intragranular fractures respectively. Intergranular fracture consumes less energy than intragranular fracture so  $K_{IC}^{inter}$  is significantly less than  $K_{IC}^{intra}$ .<sup>59</sup> The inference is then that the greater is  $A_{inter}$ , the less is  $K_{IC}$ . Earlier it was concluded that, among L-T, T-L, and S-L orientated specimens, S-L specimens had the greatest fraction of grain boundary perpendicular to the applied loading. Therefore, the fraction of intergranular fracture in S-L specimens is the highest, and S-L oriented specimens possess the least fracture toughness.

As shown in Fig. 9, level of strain or deformation induced during processing deteriorates the fracture resistance of aluminium alloys by pushing the constituents closer for L-T specimens (Fig. 2), although the influence is less than that



**9 Influence of deformation in processing on fracture toughness of aluminium alloys**



**10 Modelled dependence of fracture toughness on volume fraction and size of dispersoids**

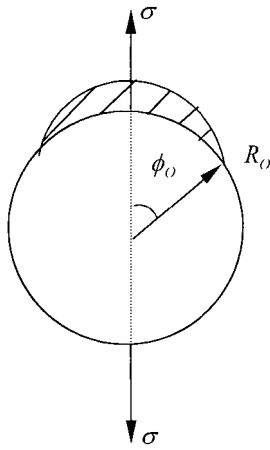
due to the presence of constituents. This may be responsible for the lower fracture toughness of work hardened metals that fail by dimpled rupture.

From the above discussions, less, smaller and equiaxed constituents are concluded to be preferable for improving the fracture toughness of aluminium alloys plates, and the L direction of the plates should be designed to endure the maximum principal external stress.

**INFLUENCE OF DISPERSOIDS ON FRACTURE TOUGHNESS**

Dispersoids provide insignificant dispersion strengthening but can influence mechanical properties indirectly because of their ability to suppress recrystallisation during product fabrication. Owing to the complicated effect, the explicit influence of dispersoids on fracture toughness is difficult to assess. Some conflicts exist among previous experimental results.<sup>61-65</sup> For instance, it is commonly believed that the void sheets, which come from decohesion of the dispersoids, truncate primary void growth and preclude large accumulations of strain, resulting in lower ductility and fracture toughness.<sup>61,62</sup> However, the presence of dispersoids has been shown to improve the fracture toughness of Al-Mg-Si alloys.<sup>63</sup> Although smaller dispersoids have been found favourable for modifying the deformation and fracture resistance of Al-Zn-Mg-Cu alloys,<sup>64</sup> larger dispersoids were also found to help to enhance the ductility of Al-Mg alloys.<sup>65</sup> Thus previous research seems to suggest that dispersoids are detrimental to fracture toughness of predominantly intragranular fracture aluminium alloys, whereas they are advantageous to predominantly intergranular fracture aluminium alloys.

Figure 10 delineates the presently modelled dependences of fracture toughness on the volume fraction and size of dispersoids on the assumption that they are arranged in a periodical cubic array. From Fig. 10 one may deduce that the influence of dispersoids on fracture toughness is not conspicuous in the industrial range of volume fraction ~0.2% and radius ~120 nm. However, increasing the volume fraction and enlarging dispersoid size are inclined to improve the ability to resist deformation and fracture. The improvement in fracture toughness by introducing more dispersoids is due to the homogenising effect of dispersoids on slip<sup>61,66</sup> and the inhibiting effect of dispersoids on grain growth and recrystallisation, which induces a fine matrix grain and furthermore a greater fraction of intragranular fracture. The reason that fracture toughness is improved by larger dispersoids may be attributed to the characteristic effect of dispersoids on fracture evolution.



**11 Micromodel of void formed by interfacial decohesion at dispersoid<sup>67</sup>**

As mentioned above, increasing the ductility/fracture of aluminium alloys by both increasing and decreasing the size of dispersoids has been observed in experiments,<sup>64,65</sup> the two conflicting trends are associated with the fracture nature of aluminium alloys. On the one hand, for aluminium fractured in a predominantly intragranular manner, the dispersoids are initiators for second voids, where void sheets are induced to promote coalescence of the primary void. Thus here the population of dispersoids is a negative factor for ductility/fracture toughness (the effect of dispersoids on controlling grain growth and recrystallisation is not considered) and the possibility of decohesion of dispersoids from the matrix determines degree of negativity. It is known that dispersoid/matrix interface decohesion occurs once the interfacial strength ( $\sigma_i$ ) exceeds a critical interfacial strength ( $\sigma_i^*$ ) that depends on particle and matrix properties.<sup>47</sup> The term  $\sigma_i$  is the sum of maximum principal stress  $\sigma_1^m$  and stress ( $\sigma_d$ ) that arises from incompatibility between a rigid, non-deforming particle and a flexible plastic matrix. The value of  $\sigma$  is given by<sup>48</sup>

$$\sigma_d = 4 \cdot 2\alpha Gb \sqrt{\rho_d} \dots \dots \dots (30)$$

where  $\alpha$  is  $1/2\pi$ ,  $G$  is shear modulus,  $b$  is the value of Burger's vector, and  $\rho_d$  has been defined earlier.  $\sigma_1^*$  can be calculated using<sup>67</sup>

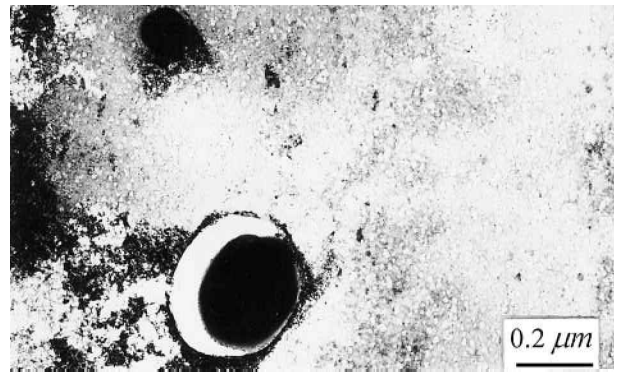
$$\sigma_1^* = \frac{1}{2} \sqrt{\left(\frac{E_m + E_d}{2}\right) \frac{(1 - \cos \phi_0)\pi\Gamma_W}{r_d(1 - \nu^2)} L_0(\phi_0)} \dots \dots (31)$$

where  $E_m$  and  $E_d$  are the modulus of matrix and dispersoids respectively,  $r_d$  is the mean radius of dispersoids,  $\phi_0$  is the half angle of incipient decohesion as sketched out in Fig. 11, and  $L_0(\phi_0)$  is a function of  $\phi_0$ ,

$$\Gamma_W = \Gamma_d + \Gamma_m - \Gamma_{dm} \dots \dots \dots (32)$$

with  $\Gamma_d$ ,  $\Gamma_m$ , and  $\Gamma_{dm}$  being the surface energy of dispersoids, matrix, and interface between dispersoids and matrix. Equation (31) clearly indicates that  $\sigma_1^*$  varies inversely with the radius of dispersoids, and larger dispersoids make it easier for decohesion to take place (Fig. 12), reducing fracture toughness in aluminium alloys.

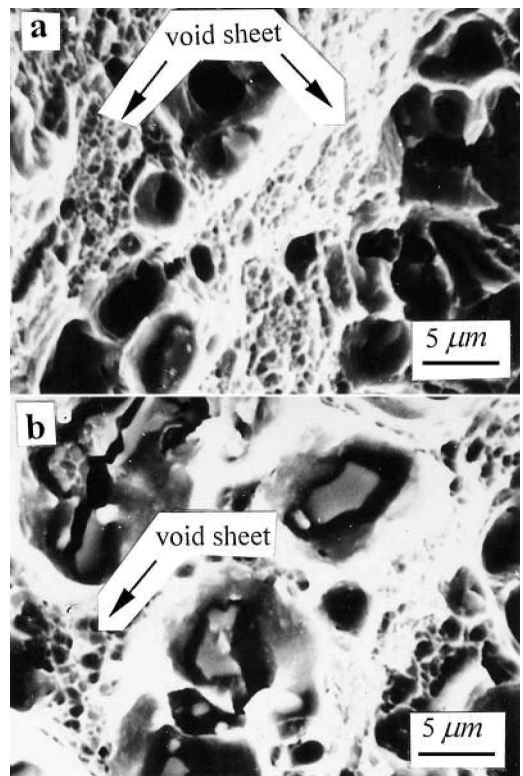
On the other hand, for aluminium fractured in a predominantly intergranular manner, suitable addition of dispersoids, through decreasing the required energy for intragranular fracture, promotes intragranular fracture thus boosting the fracture toughness. This is analogous to the microcrack toughening of ceramics. In this case, limited expansion of dispersoids is favourable for intragranular fracture, so enhancing the fracture toughness by, to some extent, preventing intergranular fracture. It is noteworthy that the size of dispersoids being discussed here is in the range



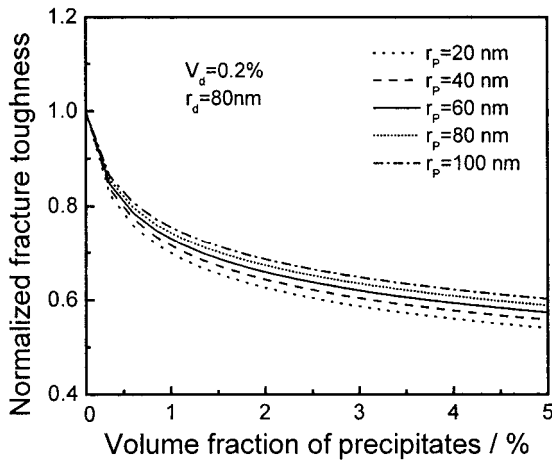
**12 TEM photograph demonstrating typical decohesion resistance of dispersoids of different sizes**

of industrial practice and the upper limit of radius is chosen as 120 nm in this model.

However, in the present experiment, dispersoids were found to enhance fracture toughness even though the fracture of specimen was predominantly intragranular. In the underaged condition, both the size and interparticle spacing of precipitates are less, so  $\rho_d$  in equation (30) follows more closely that in equation (6), which results in more dispersoids being separated from the matrix, as shown in Fig. 13a. In the peak aged condition, fewer dispersoids are separated from the matrix (Fig. 13b) because of the lower  $\rho_d$  and the more dense precipitates that consume more movable dislocations. Observing Fig. 13, it appears that the underaged specimen, having easily formed void sheets, may possess inferior fracture toughness to the peak aged specimen, in which void sheets are formed only with some difficulty. In fact, the underaged specimen possesses superior fracture toughness the increased void sheets incur a homogenous deformation that spreads over the bulk



**13 Fracture surface SEM micrographs showing morphological evolution from (a) underaged condition to (b) peak aged condition**



14 Modelled dependence of fracture toughness on volume fraction and size of precipitates

specimen. Contrarily, in the peak aged specimen under service loading, impinging of primary voids is apt to cause necking or local fracture of the specimen, resulting in a lower fracture toughness.

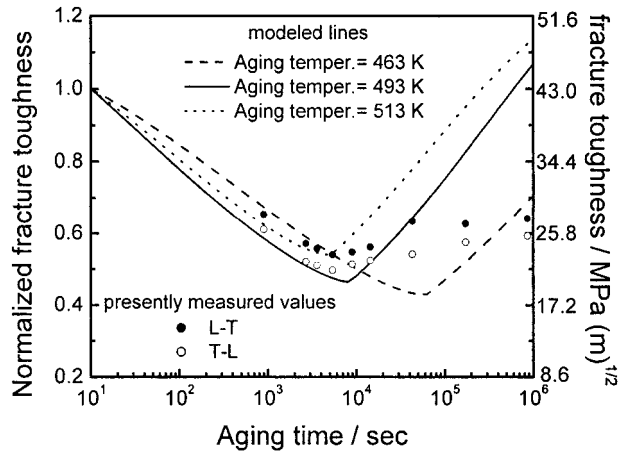
Besides the size of dispersoids, the nature of dispersoids, which is represented by  $E_d$  in equation (31), significantly affects fracture toughness. Although it is commonly accepted that the major reason for the gradual increase in fracture toughness of AA7075 containing Mn rich dispersoids, then Cr rich dispersoids, and finally Zr rich dispersoids, is the gradual decrease in size of the three dispersoids,<sup>63</sup> the influence of the characteristics of the dispersoids may be more significant. Taking the Al based binary intermetallic phase as reference, the melting temperatures of Al–Mn system dispersoids, Al–Cr system dispersoids, and Al–Zr system dispersoids, are  $\sim 820^\circ\text{C}$ ,  $\sim 940^\circ\text{C}$ , and  $\sim 2790^\circ\text{C}$ , respectively.<sup>68</sup> Because Young's modulus  $E_d$  of intermetallics is approximately linear with melting temperature,<sup>69</sup> it increases in the three kinds of dispersoids in the order Al–Mn, Al–Cr, and Al–Zr, and therefore the same order of increase results for  $\sigma_y^*$  and  $K_{IC}$ . It is thus concluded that the effect of dispersoid size on fracture toughness is entangled with other effects and may sometimes be swamped; therefore it is difficult to define independently and explicitly.

## INFLUENCE OF PRECIPITATES ON FRACTURE TOUGHNESS

Figure 14 details the dependence of fracture toughness on volume fraction and size of precipitates on the assumption that they are arranged in a periodical cubic array. It is seen that greater fracture resistance will be attained by enlarging the radius of the plate plane of precipitates  $d_p$  and specially by reducing the volume fraction of precipitates, which is the same as saying that materials possessing less strength commonly exhibit greater fracture toughness.

Although the introduction of precipitates is detrimental to fracture toughness, precipitates should not be sacrificed from the viewpoint of obtaining comprehensive mechanical properties because they provide the most significant contribution to the strength of aluminium alloys. Therefore the most effective approaches to reinforcing the fracture resistance of aluminium alloys are to decrease volume fraction and modify the shape of constituents.

It must be noted that, with changes to both volume fraction and size of precipitates, the yield strength of alloys, i.e.  $\sigma_y$  in equation (13), varies correspondingly, so that the effect of precipitates on fracture toughness is somewhat different from the effect on tensile ductility.

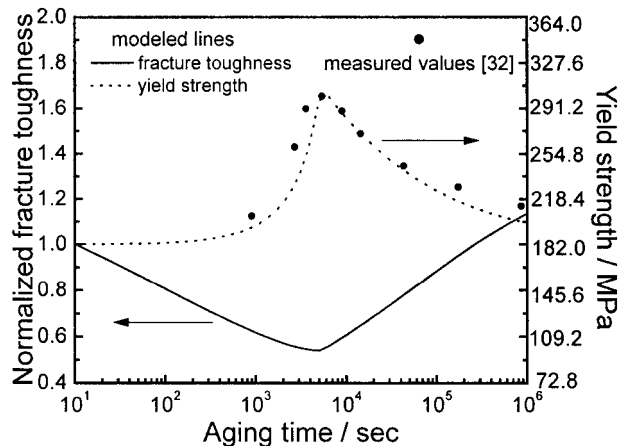


15 Variation of fracture toughness with aging time at different aging temperatures for aged Al–Cu–Mg alloy (lines are model predictions; scatters are experimentally measured values)

## FRACTURE TOUGHNESS AND YIELD STRENGTH VERSUS AGING PROCESS VARIABLES

With the advance of aging, the measured value of fracture toughness varies downwards through underaging to peakaging, and subsequently upwards during overaging. This is in approximate conformity with the predicted trend given by combining this model with the formerly constructed precipitation model of disc shaped strengthening second phases<sup>32</sup> in which the evolution of the dimensions and volume fraction of precipitates with aging as well as the variation of the corresponding strengthening effect with aging are satisfactorily simulated and could be substituted into the present model, as shown in Fig. 15. However, in the overaging case, the modelled values are much higher than measured values. This could be brought about by overestimation of the dimensions of precipitates in our kinetic modelling, as discussed in detail in Ref. 32. This results in an overestimation of  $\lambda_p$ , subsequently  $\bar{\epsilon}$ , and finally  $\epsilon$  and  $K_{IC}$  (equations (10), (11), (12) and (15)). In Fig. 16, modelled and measured variations of the most important mechanical properties, i.e. yield strength<sup>32</sup> and fracture toughness, with aging are integrated for the specimen Al–Cu–Mg alloys.

Although the variation of yield strength and fracture toughness with aging for aged aluminium alloys are essentially known from previous research,<sup>8,11,70,71</sup> Fig. 16



16 Variation of yield strength and fracture toughness with aging time at aging temperature of 513 K for aged Al–Cu–Mg alloy (lines are model predictions; scatters are experimentally measured values<sup>32</sup>)

is the first quantitatively modelled diagram (to the authors' knowledge), in spite of some discrepancy existing between modelled values and measured results. This diagram, together with some ongoing work, should be helpful for designers in understanding the conjunction of mechanical properties of aged aluminium alloys, and then in developing new aluminium alloys with optimised service ability.

## Conclusions

1. This improved model not only inherits the merits of some generally accepted fracture toughness predicting models, but also presents for the first time, a quantitative diagram illustrating the relationship between fracture toughness and yield strength during the aging of high strength aluminium alloys.

2. For fracture toughness of heat treatable aluminium alloys, the three types of second phase particles, constituents, dispersoids, and precipitates, exert seriously detrimental, less seriously detrimental, and generally beneficial influences, respectively. The key method to determine the fracture resistance is to control the constituents both in number and morphology.

3. In general, constituents and distorted grains induce the orientation effect on fracture toughness of aluminium alloys plate. Also, deformation induced during processing degrades fracture resistance.

## Acknowledgements

Financial support from State Key Project of Fundamental Research of China (Grant G1999064909) is gratefully acknowledged. The authors also wish to express their special thanks for support from the National Natural Science Foundation of China and the National Outstanding Young Investigator Grant of China.

## References

1. J. R. LOW, JR.: *Eng. Fract. Mech.*, 1968, **1**, 47–53.
2. J. G. KAUFMAN, P. E. SCHILLING and F. G. NELSON: *Met. Eng. Q.*, 1969, **9**, 39–47.
3. D. BROEK: *Eng. Fract. Mech.*, 1973, **5**, 55–66.
4. J. R. LOW, JR., R. H. VAN STONE and R. H. MERCHANT: NASA Technical Report No. 2. Research Grant NGR 38–087–003, Carnegie–Mellon University, 1972.
5. R. J. BUCCI: *Eng. Fract. Mech.*, 1979, **12**, 407–441.
6. J. T. STALEY: in 'Properties related to fracture toughness', (ed. W. R. Warke *et al.*), STP 605, 71–103; 1975, Philadelphia, PA, ASTM.
7. J. T. STALEY: *Aluminium*, 1979, **55**, 277–281.
8. G. T. HAHN and A. R. ROSENFELD: *Metall. Trans. A*, 1975, **6A**, 653–668.
9. R. H. VAN STONE and J. A. PSIODA: *Metall. Trans. A*, 1975, **6A**, 668–670.
10. G. G. GARRETT and J. F. KNOTT: *Metall. Trans. A*, 1978, **9A**, 1187–1201.
11. E. HORNBOKEN and E. A. STARKE, JR.: *Acta Metall. Mater.*, 1993, **41**, 1–16.
12. D. E. PIPER, W. E. QUIST and W. A. ANDERSON: Metallurgical Society Conf., 1966, TMS, 31, 227–280.
13. D. FIRRAO and R. ROBERTE: in 'Proc. 113th AIME Conf.', (ed. J. M. Wells and J. B. Landers), 165–177; 1985, Warrendale, PA, AIME.
14. M. NAKAI and T. ETO: *Mater. Sci. Eng. A*, 2000, **A285**, 62–68.
15. G. H. CAMPBELL, S. M. FOILES, H. HUANG, D. A. HUGHES, W. E. KING, D. H. LASSILA, D. J. NIKKEL, T. M. DE LA RUBIA, J. Y. SHU and V. P. SMYSHLYAEV: *Mater. Sci. Eng. A*, 1998, **A251**, 1–22.
16. Z. XIA, W. A. CURTIN and P. W. M. PETERS: *Acta Mater.*, 2001, **49**, 273–287.
17. A. M. GOKHALE and S. YANG: *Metall. Mater. Trans. A*, 1999, **30A**, 2369–2381.
18. J. RÖSLER and M. BAKER: *Acta Mater.*, 2000, **48**, 3553–3567.
19. N. A. FLECK and J. W. HUTCHINSON: *J. Mech. Phys. Solids*, 1993, **41**, 1825–1857.
20. N. A. FLECK and J. W. HUTCHINSON: *Adv. Appl. Mech.*, 1997, **33**, 295–361.
21. M. R. BEGLEY and J. W. HUTCHINSON: *J. Mech. Phys. Solids*, 1998, **46**, 2049–2068.
22. J. Y. SHU and N. A. FLECK: *Int. J. Solids Struct.*, 1998, **35**, 1363–1383.
23. J. Y. SHU and N. A. FLECK: *J. Mech. Phys. Solids*, 1999, **47**, 297–324.
24. H. GAO, Y. HUANG, W. D. NIX and J. W. HUTCHINSON: *J. Mech. Phys. Solids*, 1999, **47**, 1239–1263.
25. S. H. SHEN and T. C. WANG: *Acta Mater.*, 2000, **48**, 3997–4005.
26. M. E. GURTIN: *J. Mech. Phys. Solids*, 2000, **48**, 989–1036.
27. S. J. ZHOU and W. A. CURTIN: *Acta Metall. Mater.*, 1995, **43**, 3093–3104.
28. W. A. CURTIN: *Adv. Appl. Mech.*, 1999, **36**, 163–253.
29. A. TEWARI, A. M. GOKHALE and R. M. GERMAN: *Acta Mater.*, 1999, **47**, 3721–3734.
30. S. YANG, A. M. GOKHALE and Z. SHAN: *Acta Mater.*, 2000, **48**, 2307–2322.
31. Z. XUE, Y. HUANG and M. LI: *Acta Mater.*, 2002, **50**, 149–160.
32. G. LIU, G. J. ZHANG, X. D. DING, J. SUN and K. H. CHEN: *Mater. Sci. Eng. A*, 2003, **A344**, 113–124.
33. K. S. CHAN: *Acta Metall. Mater.*, 1995, **43**, 4325–4335.
34. J. W. HUTCHINSON: *J. Mech. Phys. Solids*, 1968, **16**, 13.
35. J. R. RICE and G. F. ROSENGREN: *J. Mech. Phys. Solids*, 1968, **16**, 1–12.
36. C. F. SHIH: *ASTM STP*, 1974, **560**, 187.
37. F. A. MCCLINTOCK: in 'Fundamental aspects of structural alloy design', (ed. R. I. Jaffee *et al.*), 147; 1977, New York, Wilcox, Plenum.
38. N. E. DOWLING: *Eng. Fract. Mech.*, 1987, **26**, 333–348.
39. M. F. ASHBY: *Philos. Mag.*, 1970, **21**, 399–424.
40. L. M. BROWN and W. M. STOBBS: *Philos. Mag.*, 1976, **34**, 351–372.
41. K. C. RUSSELL and M. F. ASHBY: *Acta Metall.*, 1970, **18**, 891–901.
42. G. T. HAHN and A. R. ROSENFELD: *ASTM STP*, 1968, **432**, 5–47.
43. M. J. HAYNES and R. P. GANGLOFF: *J. Test. Eval.*, 1997, **25**, 82–98.
44. J. GURLAND: in 'Quantitative microscopy', (ed. R. T. DeHoff and F. N. Rhines), 279; 1968, New York, McGraw-Hill.
45. J. W. CAHN and J. NUTTING: *Trans. ASME*, 1959, **215**, 526.
46. J. W. EDINGTON: 'Practical electron microscopy in materials science', 207; 1976, London, Van Nostrand Reinhold.
47. A. S. ARGON, J. IM and R. SAFOGLU: *Metall. Trans. A*, 1975, **6A**, 825–837.
48. S. H. GOODS and L. M. BROWN: *Acta Metall.*, 1979, **27**, 1–15.
49. J. SUN: *Eng. Fract. Mech.*, 1991, **39**, 799–805.
50. J. SUN, Z. J. DENG and M. J. TU: *Eng. Fract. Mech.*, 1990, **37**, 675–680.
51. J. GURLAND and J. PLATEAU: *Trans. Am. Soc. Metals*, 1963, **56**, 442.
52. H. TODA, T. KOBAYASHI and A. TAKAHASHI: *Mater. Sci. Eng. A*, 2000, **A280**, 69–75.
53. J. A. NOCK, JR. and H. Y. HUNSICKER: *J. Met.*, 1963, **15**, 216–224.
54. B. MORERE, J. C. EHRSTROM, P. J. GREGSON and I. SINCLAIR: *Metall. Mater. Trans. A*, 2000, **31A**, 2503–2515.
55. C. J. PEEL and P. J. E. FORSYTH: Technical Report 70162, Royal Aircraft Establishment, Farnborough, UK, September 1970.
56. N. U. DESHPANDE, A. M. GOKHALE, D. K. DENZER and J. LIU: *Metall. Mater. Trans. A*, 1998, **29A**, 1191–1201.
57. N. U. DESHPANDE, A. M. GOKHALE, D. K. DENZER and J. LIU: *Metall. Mater. Trans. A*, 1998, **29A**, 1203–1210.
58. T. KAWABATA and O. IZUMI: *Acta Metall.*, 1976, **24**, 817–825.
59. E. HORNBOKEN and M. GARF: *Acta Metall.*, 1977, **25**, 877–881.
60. M. SUGAMATA, C. P. BLANKENSHIP and E. A. STARKE, JR.: *Mater. Sci. Eng. A*, 1993, **A163**, 1–10.
61. T. B. COX and J. R. LOW, JR.: *Metall. Trans.*, 1974, **5**, 1457–1470.
62. R. H. VON STONE, T. B. COX, J. R. LOW, JR. and J. A. PSIODA: *Int. Met. Rev.*, 1985, **30**, 157–179.
63. K. C. PRINCE and J. W. MARTIN: *Acta Metall.*, 1979, **27**, 1401–1408.
64. C. Q. CHEN and J. F. KNOTT: *Met. Sci.*, 1981, **15**, 357–364.
65. S. L. LEE and S. T. WU: *Metall. Trans. A*, 1986, **17A**, 833.
66. J. A. WALSH, K. V. JATA and E. A. STARKE, JR.: *Acta Metall.*, 1989, **37**, 2861–2871.
67. J. SUN: *Int. J. Fract.*, 1990, **44**, R51–R56.

68. J. E. HATCH: 'Aluminium: properties and physical metallurgy', 140; 1984, Metals Park, Ohio, American Society for Metals.
69. M. E. FINE, L. D. BROWN and H. L. MARCUS: *Scr. Metall.*, 1984, **18**, 951–956.
70. S. SURESH, A. K. VASUDEVAN, M. TOSTEN and P. R. HOWELL: *Acta Metall.*, 1987, **35**, 25–46.
71. T. KAWABATA and O. IZUMI: *Acta Metall.*, 1981, **29**, 229–239.